Available online at www.sciencedirect.com

ScienceDirect

Acta Materialia 87 (2015) 161–173

Acta MATERIALIA

www.elsevier.com/locate/actamat

Determination of macroscopic and microscopic residual stresses in friction stir welded metal matrix composites via neutron diffraction

X.X. Zhang,[a] D.R. Ni,[a] B.L. Xiao,[a] H. Andrä,[b] W.M. Gan,[c] M. Hofmann[d] and Z.Y. Ma[a,*]

[a]*Shenyang National Laboratory for Materials Science, Institute of Metal Research, Chinese Academy of Sciences, 72 Wenhua Road, Shenyang 110016, China*

[b]*Fraunhofer Institute for Industrial Mathematics, Fraunhofer-Platz 1, Kaiserslautern 67663, Germany*

[c]*German Engineering Materials Science Centre, Helmholtz-Zentrum Geesthacht, D-21502 Geesthacht, Germany*

[d]*Technische Universität München, Forschungsneutronenquelle Heinz Maier-Leibnitz (FRM II), D-85747 Garching, Germany*

Received 17 December 2014; revised 29 December 2014; accepted 1 January 2015
Available online 27 January 2015

Abstract—This study presents a new method to determine both the macroscopic and microscopic (including elastic mismatch, thermal misfit and plastic misfit) residual stresses in metal matrix composite (MMC) welds via neutron diffraction. As an illustration, friction stir welded 17 vol.% SiCp/2009Al-T4 plates were investigated. It is shown that the calculation of the thermal misfit plus plastic misfit residual stresses in the metal matrix of the MMC welds is much more accurate by using the absolute unstrained lattice parameter of the SiC powder sample based on the stress equilibrium condition compared with using that of the unreinforced alloy sample. The profiles of the longitudinal (L), transverse (T) and normal (N) components of the total residual stress in the reinforcement are entirely different from those in the matrix. It was found that the profiles and total variations of the L, T and N components of the total residual stress are dominated by those of the macroscopic residual stress in the matrix, and by those of the elastic mismatch residual stress in the reinforcement, revealing a significant load transfer from the matrix to the reinforcement. The maximum total residual stress in the metal matrix of the FSW 17 vol.% SiCp/2009Al-T4 weld could reach up to ~69% of the yield strength of the 2009Al-T4 alloy. Increasing the rotation rate has small effects on the basic profiles of the total residual stress, apart from increasing the width of the profiles.

Keywords: Residual stress; Metal matrix composites; Neutron diffraction; Friction stir welding

1. Introduction

Metal matrix composites (MMCs) possess greater stiffness and strength, improved resistance to fatigue, wear and creep, a lower coefficient of thermal expansion (CTE) and better dimension stability compared to unreinforced metals, which makes MMCs the ideal structural materials for aerospace and defense applications. However, the high manufacturing cost, the poor formability and weldability of MMCs are the major factors that limit the widespread application of MMCs [1].

Friction stir welding (FSW), an innovative solid-state joining technique, is considered to be a promising technique to produce high quality MMC welds. In the early stage of applying FSW to MMCs, due to the poor flow ability of material and the severe tool wear, welding defects were easy to form in the welds, such as the surface defects [2], the matrix voids [3,4], the particle cracks [5], and the impurities resulting from the tool wear [2,6]. In recent years, with the development of new types of welding tools, such as the WC/Co tool coated with diamond [7] and the ultra-hard cermet tool [8], sound MMC welds can be produced via FSW under careful design of the welding parameters [9,10].

As with other welding processes, residual stresses are generated after FSW. Early in FSW development, the residual stress in FSW joints was thought to be very small compared to that in fusion welded joints [11], however, in recent years further research has revealed that the residual stress in FSW joints can be significant [12–20]. For instance, the ratio of the maximum longitudinal (L) residual stress to the yield strength of the base material ranges from ~20% to 99% in FSW aluminum alloys [18–20]. Residual stress in the welds is a crucial issue because it significantly affects the weld performance [21–25], such as plastic collapse [21,25], fatigue properties [23,24] and stress corrosion [26]. To guarantee the safety of engineering design, improve the accuracy of life prediction and damage evolution models for highly reliable structures, accurate knowledge of the residual stress in the welds is crucial.

Until now, there have been only limited studies on the residual strain or stress in MMC welds using

* Corresponding author. Tel./fax: +86 24 83978908; e-mail: zyma@imr.ac.cn

http://dx.doi.org/10.1016/j.actamat.2015.01.006
1359-6462/

non-destructive measurements [22,27,28]. For instance, Jun et al. [27] measured the residual stress in linear friction welded 25 vol.% SiCp/2124Al plate via neutron diffraction. The unstrained lattice parameters were roughly obtained through the measurements at the corner of the plate, however, because strain-free samples were unavailable [27]. This introduced significant errors because the variations of the unstrained lattice parameter of the 2124Al matrix due to thermal exposure were not taken into account. Other investigators [22,28] measured the residual stress in small samples cut from MMC welds. Due to stress relaxation, the measured residual stresses were found to be small [22,28]. An unexpected profile of the residual stress that was measured using traditional X-ray diffraction was also detected due to uncertain surface effects [22]. No systematic study has been undertaken to investigate the residual stress in MMC welds.

According to their scales and sources, the residual stresses in MMCs are divided into macroscopic and microscopic (including elastic mismatch, thermal misfit and plastic misfit) residual stresses [29]. The macroscopic residual stress has a variation wavelength at the scale of several millimeters or more. The elastic mismatch residual stress, reflecting the load transfer from the matrix to the reinforcement, is the result of the mismatch in elastic constants between the matrix and the reinforcement. The thermal misfit plus plastic misfit residual stresses arise during cooling because of the mismatch in the CTE between the two phases. The plastic misfit residual stress is generated because plastic deformation occurs in the ductile matrix, while only elastic deformation takes place in the stiff reinforcement. The plastic deformation in the matrix can be caused by the macroscopic temperature gradient, the stirring effect of the welding tool and the heterogeneous deformation during the cooling stage of the FSW process due to the mismatch in the CTE between the matrix and the reinforcement. The elastic mismatch, thermal misfit and plastic misfit residual stresses are phase specific and belong to the microscopic residual stress, with a variation wavelength at the scale of several micrometers. Clearly, the residual stress in MMCs is more complex than that in unreinforced metals. Consequently, current methods of determining the residual stress for unreinforced metals have their limitations for MMC welds.

Recently, Cioffi et al. [20] proposed a method to determine the macroscopic residual stress in unreinforced metals based on a genetic algorithm and equilibrium conditions of both stress and bending moments, avoiding measuring the unstrained reference parameter. So far, applying this new method [20] to MMCs remains a great challenge and the process needs further development. The complexities induced by the load transfer from the matrix to the reinforcement and the presence of the thermal misfit plus plastic misfit residual stresses have to be taken into account. To solve these issues, the measurements of the unstrained reference lattice parameters may be unavoidable. Besides, further hypotheses about these methods may be necessary. For instance, the elastic mismatch, thermal misfit and plastic misfit residual stresses may be assumed to be constant across the weld, and then, the problem is virtually the same as exists without reinforcement. In spite of this, the measurements of the unstrained reference lattice parameters for the metal matrix of MMCs are especially difficult [30], because the precipitation state in the matrix is changed due to the non-uniform thermal histories. Such variations of the precipitation state lead to changes in the unstrained reference lattice parameters according to Vegard's law [31]. So far, there is no report of applying these methods to ascertain the macroscopic and phase specific microscopic residual stresses in MMC welds.

To sum up, there is a strong demand to develop a new framework to measure, separate and analyze the macroscopic and phase specific microscopic (including elastic mismatch, thermal misfit and plastic misfit) residual stresses in each phase of MMC welds and such a framework is the main contribution of the present work. The effects of the rotation rate on the residual stress in FSW MMC welds are also assessed. The residual stresses in FSW 17 vol.% SiCp/2009Al-T4 plates are studied as an example.

2. Experiments

2.1. Material and FSW

3.1 mm thick 17 vol.% SiCp/2009Al-T4 composite plates were used in the present work. 2009Al alloy has a nominal composition of Al–4.0Cu–1.4Mg (wt.%) and SiC particles have an average size of 7 μm. The composite was fabricated using the powder metallurgy (PM) technique and subsequently hot rolled into plates at 480 °C. The detailed fabrication and rolling processes have been described in a previous study [22]. The composite plates were heat treated to T4 condition (solution treated at 516 °C for 1 h, water quenched and naturally aged for 7 days).

Composite plates $300 \times 75 \times 3.1\ mm^3$ in size were welded parallel to the rolling direction, at a welding speed of 100 mm/min with rotational rates of 600 and 1500 rpm. A cermet tool with a shoulder 14 mm in diameter and a cylindrical pin 5 mm in diameter and 2.7 mm in length was adopted. The FSW MMC samples are named R600 (600 rpm) and R1500 (1500 rpm), respectively. The detailed information about FSW of the composites was reported in the previous investigations [8,9,22,32–34]. Optical microscopic (OM) examination was carried out on the transverse section of the welds. The OM specimens were mechanically polished and etched by Keller's reagent.

2.2. Neutron diffraction

Neutron diffraction at the diffractometer STRESS-SPEC of FRM II [35] was used to measure the three principal strains, along the L, transverse (T) and normal (N) directions, across the welds at the middle thickness and the middle weld length (see Fig. 1). The Si monochromator was selected using symmetric (400) reflection yielding a wavelength of $\lambda = 1.7458$ Å for the neutron diffraction. This wavelength enabled simultaneous measurement of the 2009Al (311) and 6H SiC (116) reflections at scattering angles of $2\theta_{Al} \sim 91°$ and $2\theta_{SiC} \sim 83°$, respectively.

The states of the residual stress in different samples should be understood for extracting different residual strains. Usually a comb sample, in which the macroscopic residual stress is assumed to be relaxed, is used to determine the unstrained reference lattice parameter d_0 for calculating the macroscopic residual strains in welded samples [36]. In MMCs, the macroscopic residual stress will create additional microscopic residual stress due to the mismatch in stiffness, i.e. the elastic mismatch residual stress. Taking this into account, the elastic mismatch residual stress is therefore also assumed to be relaxed in the comb samples.

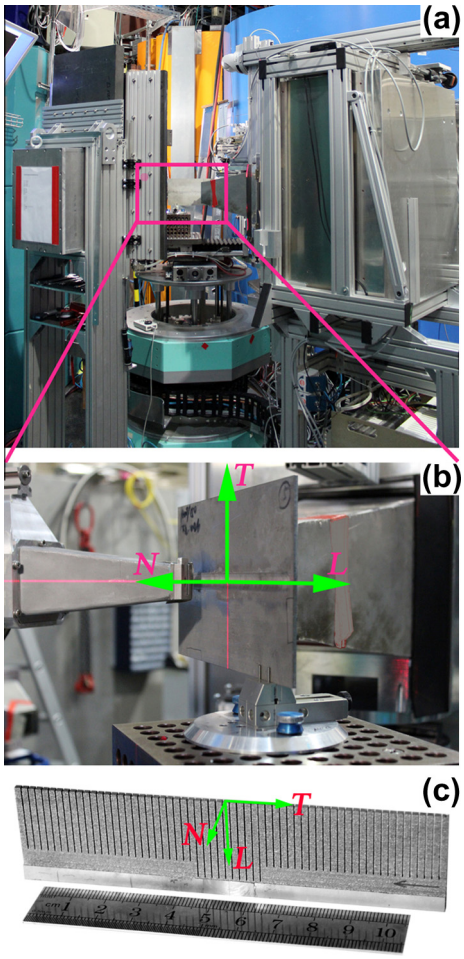

Fig. 1. Pictures of (a) the diffractometer STRESS-SPEC of FRM-II, (b) experiment setup and definition of coordinate system, and (c) comb sample for measuring the macroscopic plus elastic mismatch residual strains free parameters $d_0^{m,M+eM}$ and $d_0^{p,M+eM}$.

In this regard, only the thermal misfit plus plastic misfit residual stresses remain in the comb samples of MMC welds, so the macroscopic plus elastic mismatch residual strains can be extracted by calculating the relative differences in the lattice parameters between the welded and comb MMC samples.

In the present work, two FSW MMC samples, R600 and R1500, and the two corresponding comb samples, R600-ref and R1500-ref, were measured. The lattice parameters of the matrix and reinforcement measured from the FSW MMC samples are written as d^m and d^p, respectively, where the superscripts m and p denote the matrix and the reinforcement, respectively. The lattice parameters of the matrix and the reinforcement measured from R600-ref and R1500-ref are written as $d_0^{m,M+eM}$ and $d_0^{p,M+eM}$, respectively, where the superscript M denotes macroscopic, eM elastic mismatch.

In order to estimate the thermal misfit plus plastic misfit residual stresses in the reinforcement, one SiC powder sample was measured to find the 'absolute unstrained reference' parameters $d_0^{p,a}$, where the superscript a denotes absolute. The thermal misfit plus plastic misfit residual strain in the reinforcement can be extracted by calculating the relative differences in the lattice parameters between the comb MMC samples and the SiC powder samples. The thermal misfit plus plastic misfit residual stresses in the matrix can be calculated from the ones in the reinforcement using the equilibrium condition of microscopic residual stresses. For the purpose of comparison, a cubic sample of the unreinforced 2009Al alloy was also measured to determine a rough 'absolute unstrained reference' lattice parameter $d_0^{m,a}$, from which the thermal misfit plus plastic misfit residual strains in the matrix can be roughly calculated.

Fig. 1(a) shows the experiment setup in STRESS-SPEC of FRM II. The picture detail in Fig. 1(b) shows the definition of the coordinate system for the FSW MMC samples. The origin of the coordinate system is located at the geometrical center of the FSW MMC sample. The positive T direction is on the advancing side of the FSW MMC sample. Fig. 1(c) shows the comb sample which had a dimension of $30 \times 122 \times 1.8\ \text{mm}^3$. Around ± 9 mm of the weld center (T direction) each tooth had a dimension of $25 \times 1.8 \times 1.8\ \text{mm}^3$, and beyond ± 9 mm (T direction) positions each tooth had a dimension of $20 \times 1.8 \times 1.8\ \text{mm}^3$, with the inter-teeth distance of 0.2 mm.

The gauge volumes for measuring the L, T and N components of the residual strains of R600 and R1500 were $2 \times 2 \times 1$, $20 \times 1 \times 1$, and $1 \times 20 \times 1\ \text{mm}^3$. The gauge volume for measuring $d_0^{m,M+eM}$ and $d_0^{p,M+eM}$ of R600-ref and R1500-ref was $10 \times 1 \times 1\ \text{mm}^3$.

The raw diffraction data were analyzed using StressTextureCalculator (STeCa) software [37] to extract the scattering angle 2θ of diffraction peaks. The total residual strains $\varepsilon_i^{\beta,\text{total}}$ are then calculated using

$$\varepsilon_i^{\beta,\text{total}} = \frac{d_i^\beta - d_0^{\beta,a}}{d_0^{\beta,a}} = \frac{\sin\theta_0^{\beta,a}}{\sin\theta_i^\beta} - 1 \tag{1}$$

where the superscript β denotes each phase in MMCs ($\beta = m$ or p), the subscript i the tensor component ($i = L$, T or N), d_i^β are the lattice parameters of the FSW MMC samples, $d_0^{\beta,a}$ the lattice parameters of 'absolute unstrained reference' samples, $\theta_0^{\beta,a}$ the diffraction angles of 'absolute unstrained reference' samples, and θ_i^β the diffraction angles of the FSW MMC samples.

The macroscopic plus elastic mismatch residual strains $\varepsilon_i^{\beta,M+eM}$ are calculated using:

$$\varepsilon_i^{\beta,M+eM} = \frac{d_i^\beta - d_0^{\beta,M+eM}}{d_0^{\beta,M+eM}} = \frac{\sin\theta_0^{\beta,M+eM}}{\sin\theta_i^\beta} - 1 \tag{2}$$

where $d_0^{\beta,M+eM}$ is the lattice spacing of comb samples, and $\theta_0^{\beta,M+eM}$ the diffraction angles of the comb samples.

The thermal misfit plus plastic misfit residual strains $\varepsilon_i^{\beta,tM+pM}$ are assumed to be isotropic and are calculated using:

$$\varepsilon_i^{\beta,tM+pM} = \frac{d_i^{\beta,M+eM} - d_0^{\beta,a}}{d_0^{\beta,a}} = \frac{\sin\theta_0^{\beta,a}}{\sin\theta_i^{\beta,M+eM}} - 1 \tag{3}$$

where the superscript tM denotes thermal misfit and pM plastic misfit.

3. Experimental results

3.1. Microstructures

Figs. 2(a) and 3(a) show that no defect was detected in both R600 and R1500, indicating that sound welds

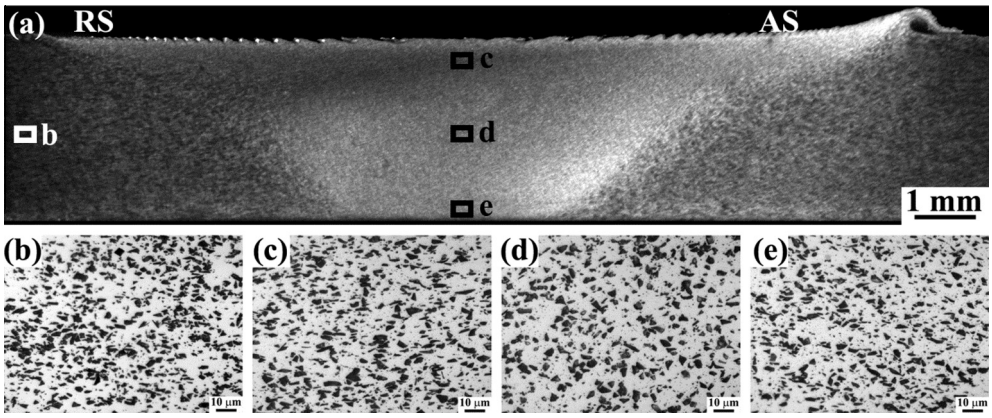

Fig. 2. Optical images of R600: (a) macrograph of the weld, (b) base material, (c) top of nugget zone, (d) center of nugget zone, (e) bottom of nugget zone. The locations of (b)–(e) are shown in (a) (RS: retreating side and AS: advancing side).

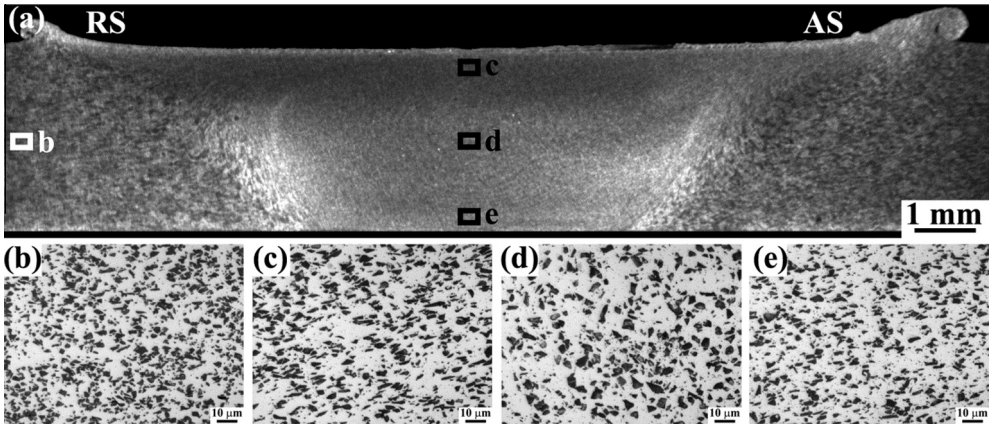

Fig. 3. Fig. 2 Optical images of R1500: (a) macrograph of the weld, (b) base material, (c) top of nugget zone, (d) center of nugget zone, (e) bottom of nugget zone. The locations of (b)–(e) are shown in (a) (RS: retreating side and AS: advancing side).

could be achieved via FSW at rotation rates of 600 and 1500 rpm. It is noted that no onion structure was observed in the nugget zone (NZ) for R600, whereas the onion structure was visible for R1500. Yan et al. [38] also showed that the onion structure appeared in the NZ at higher rotation rates due to stronger stirring effects of the welding tool.

Figs. 2(b)–(e) and 3(b)–(e) show that particle clusters in the BM were broken up and the particle distribution in the NZ was homogeneous for both R600 and R1500, in agreement with previous studies [8,9,22,32–34]. Figs. 2(d) and 3(d) show that unlike those in the top and bottom of the NZ, the SiC particles in the center of the NZ tended to align along the vertical direction (the *N* direction), in agreement with previous studies [9,22]. Besides, it can be seen that more SiC particles aligned along the *N* direction for R1500 compared to R600.

3.2. Residual strains

Fig. 4 shows the results of macroscopic plus elastic mismatch residual strain $\varepsilon_i^{\beta,M+eM}$ in the half-thickness across the weld for R600 and R1500. Fig. 4(a) shows that in the 2009Al matrix the profiles of $\varepsilon_L^{m,M+eM}$ are approximately M-shaped, in agreement with previous results [20,39–41]. The total variations of $\varepsilon_L^{m,M+eM}$ are ~2300 $\mu\varepsilon$ for both R600 and R1500. Fig. 4(b) shows that in the SiC reinforcement the profiles of $\varepsilon_L^{p,M+eM}$, unlike those of $\varepsilon_L^{m,M+eM}$, have three peaks. The values away from the weld are ~0 $\mu\varepsilon$. The highest values of $\varepsilon_L^{p,M+eM}$ are found at the weld center and are ~520 $\mu\varepsilon$ for both R600 and R1500. Fig. 4(c) shows that in the 2009Al matrix the total variations of $\varepsilon_T^{m,M+eM}$ are ~850 and ~730 $\mu\varepsilon$ for R600 and R1500, respectively. Fig. 4(d) shows that in the SiC reinforcement the total variations of $\varepsilon_T^{p,M+eM}$ increase from ~420 to ~730 $\mu\varepsilon$ when increasing the rotation rate from 600 to 1500 rpm. Fig. 4(e) shows that in the 2009Al matrix the profiles of $\varepsilon_N^{m,M+eM}$ were approximately W-shaped, with total variations of about 1000 $\mu\varepsilon$. Fig. 4(f) shows that in the SiC reinforcement the profiles of $\varepsilon_N^{p,M+eM}$ are V-shaped, with the lowest value located approximately at the weld center. The lowest values of $\varepsilon_N^{p,M+eM}$ are about −180 and −460 $\mu\varepsilon$ for R600 and R1500, respectively.

Fig. 5 shows the results of the measured total residual strains $\varepsilon_i^{\beta,\text{total}}$ for both R600 and R1500. The difference between the total residual strain and the macroscopic plus elastic mismatch residual strain is caused by the thermal misfit plus plastic misfit residual strains.

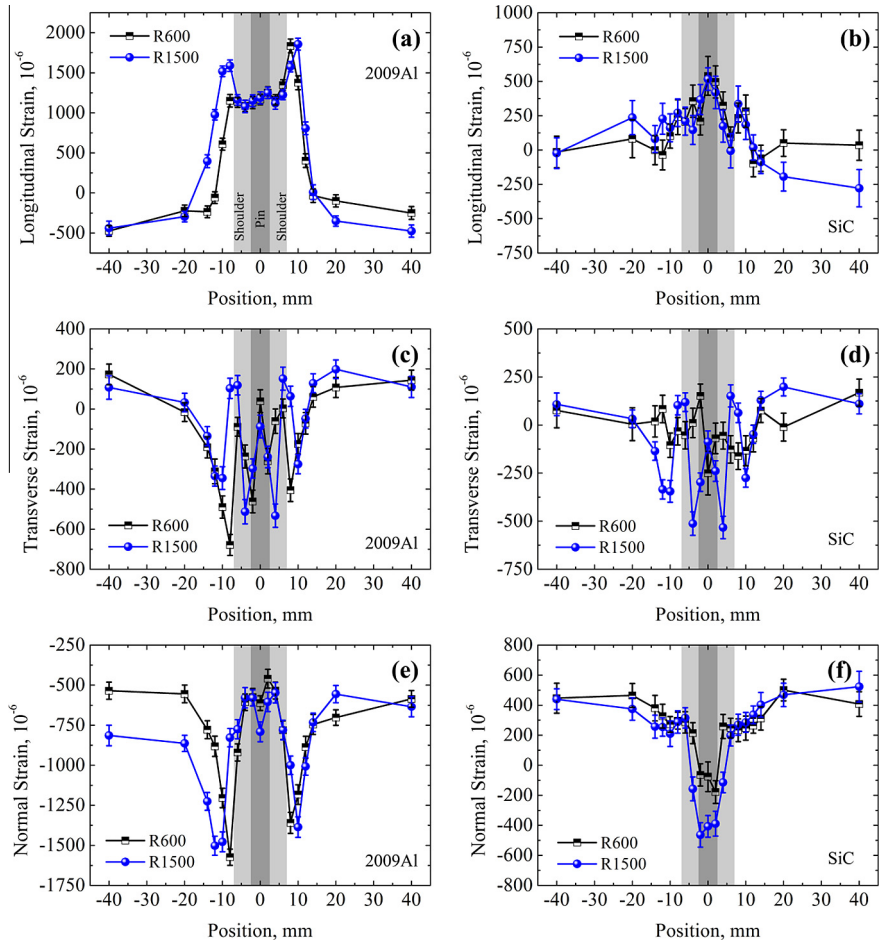

Fig. 4. Comparison of the profiles of the L, T and N components of measured macroscopic plus elastic mismatch residual strains across the welds at the middle thickness and middle weld length for R600 and R1500: (a) L, (c) T and (e) N components in the 2009Al matrix, (b) L, (d) T and (f) N components in the SiC reinforcements.

4. Analysis and discussion

4.1. The unstrained reference lattice parameters

The variation of $d_0^{m,M+eM}$ in the matrix measured from the comb sample is mainly caused by five factors: the remaining macroscopic residual stress, the thermal misfit residual stress, the plastic misfit residual stress, the variation of the precipitation state and the inter-granular residual stress. The variation of $d_0^{p,M+eM}$ in the reinforcement measured from the comb sample is mainly caused by the remaining macroscopic residual stress, the thermal misfit residual stress and the plastic misfit residual stress. For ceramic reinforcement, there is no precipitation, thus, no variation of the precipitation state.

Generally, the remaining macroscopic residual stress in the comb sample is small and does not lead to a large error in the final stress calculation [19,36,42]. Previous investigation [43] showed that the remaining macroscopic residual stress at the weld center was approximately zero, however, the remaining macroscopic residual stress was reported to be ~10 MPa at positions ±20 mm away from the weld center, and increased to ~20 MPa at positions ±40 mm away from the weld center [43]. Such remaining macroscopic residual stress was probably caused by the large cross-section of tooth (2.7×2.7 mm^2) and the short tooth length (8 mm) [43].

It is known that the magnitude of the remaining macroscopic residual stress depends on the sample size [24,44], therefore, decreasing the dimension of the cross-section of each tooth can reduce the remaining macroscopic residual stress considerably. In the present study, to minimize the remaining macroscopic residual stress in the comb sample, each tooth was designed to have a dimension of 1.8×1.8 mm^2 for its cross-section, just about 45% in the area of the comb sample used as a reference in [43].

In addition, each tooth for the comb samples is connected to the comb bottom for making the measurements at different positions easier. To reduce the effect of the comb bottom, the length of each tooth should be long and the positions of measurements should be as close as possible to the end of the tooth [42]. In this study, the length of each tooth was 25 mm within ±9 mm positions from the weld center and that was 20 mm beyond ±9 mm positions from the weld center, which were much longer than that (8 mm) in reference [43]. It is therefore reasonable to assume that the influence of the remaining macroscopic residual stresses in the comb samples was smaller than that of earlier studies.

The thermal misfit residual stress should be hydrostatic [29]. When the composite is cooled down from a high temperature (e.g. welding or heat treatment temperature), the thermal misfit residual stress is tensile in the 2009Al matrix and compressive in the SiC reinforcement, which is the

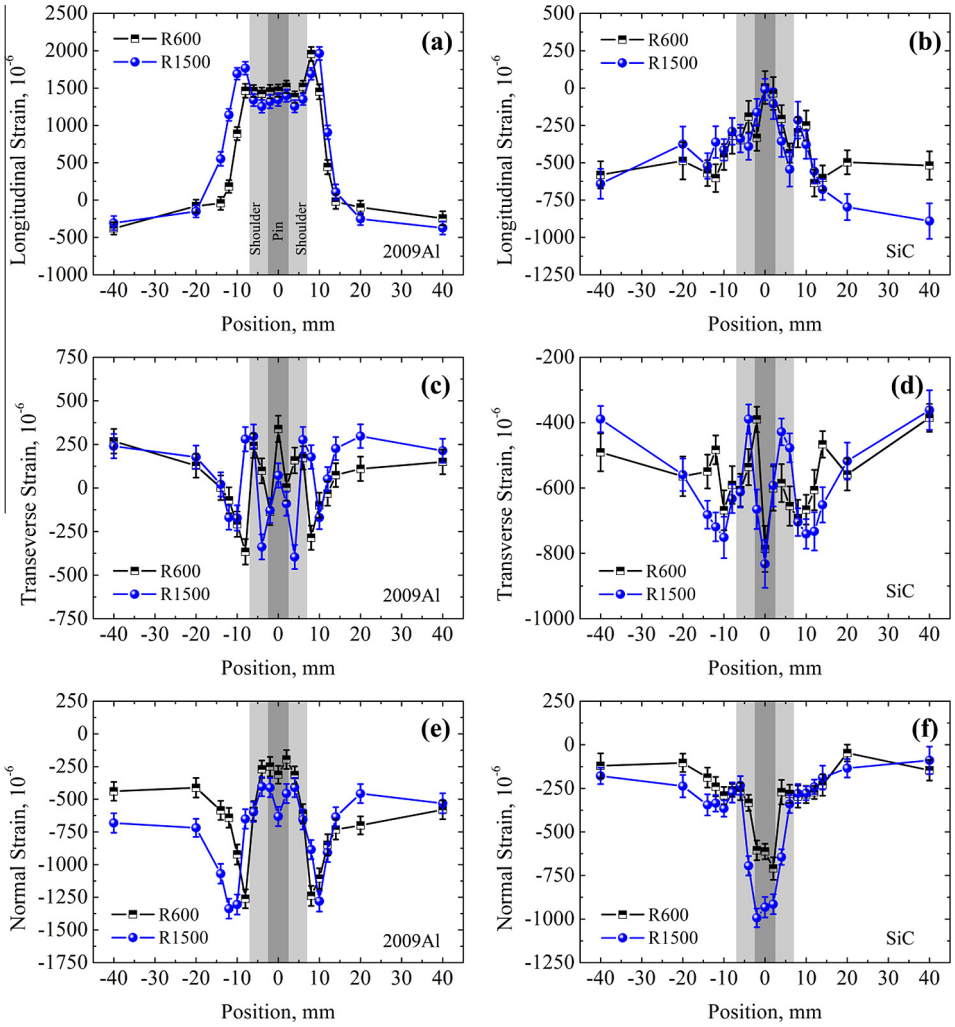

Fig. 5. Comparison of the profiles of the L, T and N components of measured total residual strains across the welds at the middle thickness and middle weld length for R600 and R1500: (a) L, (c) T and (e) N components in the 2009Al matrix, (b) L, (d) T and (f) N components in the SiC reinforcements.

usual behavior in MMCs with ductile Al matrix and stiff particles [29]. Accurate determination of thermal misfit residual stress in the 2009Al matrix of the FSW MMC welds requires one sample of FSW unreinforced 2009Al weld, which must be of exactly the same chemical composition and precipitation state as those in the matrix of the FSW MMC welds. This is impossible for the following reasons. Firstly, the thermal history of the whole FSW composite plate is unknown. Secondly, even if a FSW unreinforced alloy weld can be reproduced so that it experiences exactly the same thermal history everywhere throughout the sample, as the corresponding FSW MMCs, the FSW unreinforced alloy weld does not have the same precipitation state as that in the matrix of the FSW MMC welds. This is because the precipitation behavior in the matrix of MMCs is different from that in the unreinforced alloy due to the presence of the reinforcement [45].

The plastic misfit residual stress results from heterogeneous plastic deformation [21]. For MMCs, the ductile matrix may experience plastic deformation, while the stiff reinforcement only experiences elastic deformation. The plastic deformation in the matrix due to the macroscopic temperature gradient and the stirring effect of the welding tool mainly occurs in the NZ [46]. This would lead to generation of plastic misfit residual stress. Nonetheless, it should be noted that dynamic recrystallization during FSW will more or less sweep away the dislocations generated by the plastic deformation. Hence, the plastic misfit residual stress that is caused by the macroscopic temperature gradient and the stirring effect of the welding tool is assumed to be zero after dynamic recrystallization. Hence, the plastic misfit residual stress is mainly caused by the heterogeneous deformation during the cooling stage of the FSW process due to the mismatch in the CTE between the matrix and the reinforcement, and can be assumed to be isotropic.

To obtain accurate values of the thermal misfit plus plastic misfit residual stresses in the 2009Al matrix, the stress equilibrium condition of the microscopic residual stresses between the 2009Al matrix and the SiC reinforcement can be applied:

$$(1-V)\sigma^{m,tM+pM} + V\sigma^{p,tM+pM} = 0 \tag{4}$$

where V is the volume content of the reinforcement. The thermal misfit plus plastic misfit residual stresses in the SiC reinforcement can be calculated directly using the value

from the powder reference sample, $d_0^{p,a}$, which leads to Eq. (5). Note that any remaining macroscopic residual stress may cause some mild errors.

$$\sigma^{p,tM+pM} = 3K^p \varepsilon^{p,tM+pM} = 3K^p \frac{d_0^{p,M+eM} - d_0^{p,a}}{d_0^{p,a}} \quad (5)$$

where K is the bulk modulus. The relationship between $\sigma^{m,tM+pM}$ and $d_0^{m,a}$ is written as

$$\sigma^{m,tM+pM} = 3K^m \varepsilon^{m,tM+pM} = 3K^m \frac{d_0^{m,M+eM} - d_0^{m,a}}{d_0^{m,a}} \quad (6)$$

Inserting Eqs. (5) and (6) into Eq. (4), and rearranging the equation, one can recalculate $d_0^{m,a}$ in terms of $d_0^{p,a}$ by

$$d_0^{m,a} = (1-V)K^m d_0^{m,M+eM} \left[(1-V)K^m - VK^p \frac{d_0^{p,M+eM} - d_0^{p,a}}{d_0^{p,a}} \right]^{-1} \quad (7)$$

The values of the calculated $d_0^{m,a}$ based on $d_0^{p,a}$ for R600 and R1500 are shown in Fig. 6(a) and (c), respectively.

Variation in the precipitation state in the 2009Al matrix is another factor in variations of $d_0^{m,M+eM}$. For age-hardened alloys, welding thermal history leads to phase transformation [8,32]. Ni et al. [32] showed that for the base material (BM) of the SiCp/2009Al-T351 composite, only a few S (Al_2CuMg) precipitates and Mg_2Si impurities were observed in the 2009Al matrix. For the FSW sample of the SiCp/2009Al-T351 composite, at a rotation rate of 1000 rpm and a welding speed of 50 mm/min, significant amounts of θ (Al_2Cu) and S (Al_2CuMg) phases precipitated out in the HAZ, and some θ (Al_2Cu) phase precipitated out in the NZ [32]. The effects of the Cu and Mg atoms on the lattice parameter a (10^{-10} m) of Al are described by Vegard's law [31,47]:

$$a = 4.04946 - 0.00480 x_{Cu} \quad (8)$$

$$a = 4.04946 + 0.00374 x_{Mg} \quad (9)$$

where x_{Cu} and x_{Mg} are the solute content (at.%) of the Cu and Mg atoms, respectively.

Taking into account Eqs. (8) and (9), it is clear that the lattice parameter of the 2009Al matrix recovers (increases compared to that of BM) with the formations of θ (Al_2Cu) and S (Al_2CuMg) phases. This explains the variation trend in the calculated $d_0^{m,a}$ for R600-ref and R1500-ref in Fig. 6(a) and (c). The difference in the $d_0^{m,a}$ between R600-ref and R1500-ref can be explained by the variation of welding heat input, which changed the precipitation sequences and resulted in different precipitation states.

The calculated 'absolute unstrained reference' $d_0^{m,a}$ suggests that the variation of precipitation states in the weld zone leads to a strain of around 221 and 77 $\mu\varepsilon$ in the 2009Al (311) plane for R600 and R1500, respectively. The relationship between the strain in the inter-planar spacing of the (hkl) planes, ε_{hkl}, and the strain in the lattice parameter A, ε_A is written as [48]:

$$\varepsilon_{hkl} = \frac{\varepsilon_A}{\sqrt{h^2+k^2+l^2}} \quad (10)$$

Using Eq. (10), it is easy to calculate that the variations of precipitation states results in a lattice strain ε_A of around 733 and 255 $\mu\varepsilon$ for R600 and R1500, respectively.

The final factor that may possibly cause a variation of $d_0^{m,M+eM}$ for the 2009Al matrix is the inter-granular residual stress, which is microscopic. For MMCs, the inter-granular residual stress arises in the matrix in the manufacturing process, e.g. rolling, because of the anisotropy of elastic constants and plastic deformation behavior. Existence of anisotropic plastic deformation is reflected by the

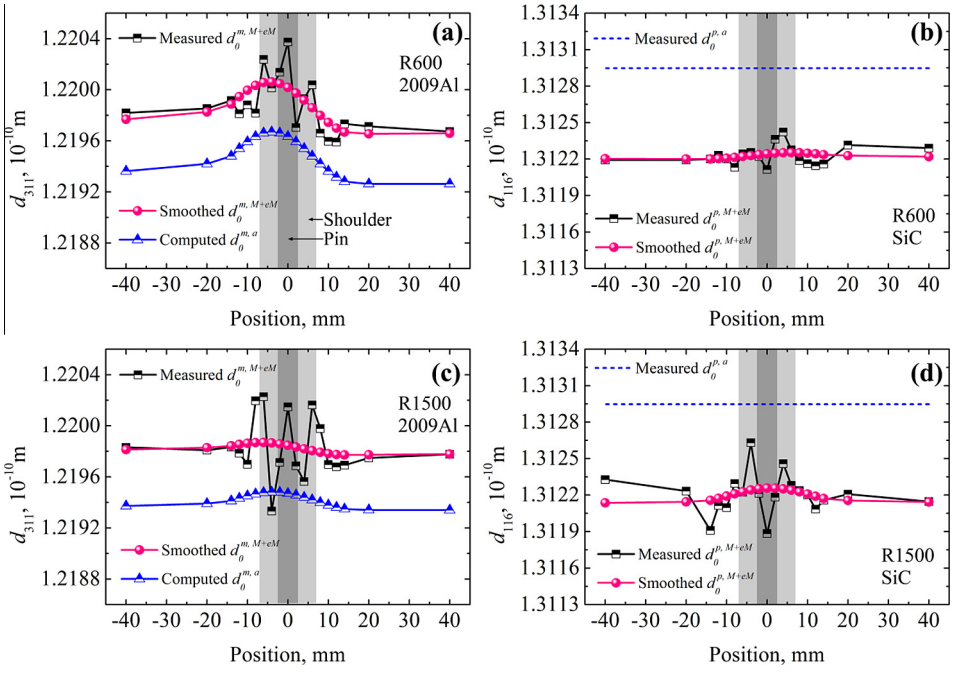

Fig. 6. The inter-planar spacing of different unstrained reference samples for R600 and R1500: (a) and (c) d_{311} of the 2009Al matrix, 'measured $d_0^{m,M+eM}$' is determined from the comb samples, 'smoothed $d_0^{m,M+eM}$' is smoothed from the 'measured $d_0^{m,M+eM}$', 'computed $d_0^{m,a}$' is calculated via Eq. (7); (b) and (d) d_{116} of the SiC reinforcements, 'measured $d_0^{p,M+eM}$' is determined from the comb samples, 'smoothed $d_0^{p,M+eM}$' is smoothed from the 'measured $d_0^{p,M+eM}$', 'measured $d_0^{p,a}$' is determined from the SiC powder sample.

generation of local textures in the FSW welds [49,50]. Although the inter-granular residual stress may affect the measurements of comb samples, the effects are small. This is supported by several recent studies [20,42,43] which revealed that the magnitude of the inter-granular residual stress is insignificant.

4.2. Extraction of macroscopic and microscopic residual stresses

The diffraction elastic constants that are calculated using software ISODEC [51] are used to extract the residual stresses from the measured residual strains. Using ISODEC, $E = 72.5$ GPa and $\nu = 0.343$ are determined for the 2009Al (3 1 1) reflection, whereas $E = 430.5$ GPa and $\nu = 0.175$ are determined for the 6H SiC (1 1 6) reflection.

To separate the macroscopic residual stress from the elastic mismatch residual stress, the stress equilibrium condition of $\sigma_i^{\beta,eM}$ over one gauge volume can be applied,

$$(1-V)\sigma_i^{m,eM} + V\sigma_i^{p,eM} = 0 \tag{11}$$

The macroscopic residual stress which is the same in each phase can then be calculated using:

$$\sigma_i^{M} = (1-V)\sigma_i^{m,M+eM} + V\sigma_i^{p,M+eM} \tag{12}$$

$$\sigma_i^{\beta,M+eM} = \sigma_i^{M} + \sigma_i^{\beta,eM} \tag{13}$$

where $\sigma_i^{\beta,M+eM}$ is the macroscopic plus elastic mismatch residual stress that can be calculated from $\varepsilon_i^{\beta,M+eM}$. The elastic mismatch residual stress is then calculated via

$$\sigma_i^{\beta,eM} = \sigma_i^{\beta,M+eM} - \sigma_i^{M} \tag{14}$$

The thermal misfit plus plastic misfit residual stresses $\sigma^{\beta,tM+pM}$ are assumed to be hydrostatic stresses. $\sigma^{p,tM+pM}$ can be calculated by Eq. (5) directly, whereas $\sigma^{m,tM+pM}$ can be roughly calculated from Eq. (6), however, significant errors would be introduced into $\sigma^{m,tM+pM}$ by using the measured $d_0^{m,a}$ directly. $\sigma^{m,tM+pM}$ can be calculated more precisely via $\sigma^{p,tM+pM}$ based on the stress equilibrium condition, through Eq. (4). In this regard, $\sigma^{m,tM+pM}$ is written in terms of $d_0^{p,a}$ by Eq. (15).

$$\sigma^{m,tM+pM} = \frac{V}{V-1}\sigma^{p,tM+pM} = \frac{3VK^p}{V-1}\frac{d_0^{p,M+eM} - d_0^{p,a}}{d_0^{p,a}} \tag{15}$$

The total residual stress can then be obtained by summing up σ_i^{M}, $\sigma_i^{\beta,eM}$ and $\sigma^{\beta,tM+pM}$.

4.2.1. The thermal misfit plus plastic misfit residual stresses

Fig. 7(a) shows the thermal misfit plus plastic misfit residual stresses $\sigma^{m,tM+pM}$ for both rotation rates calculated both via Eq. (6) using the directly measured $d_0^{m,a}$ and via Eq. (15) using $d_0^{p,a}$. The thermal misfit plus plastic misfit residual stresses calculated using $d_0^{m,a}$ show significant asymmetry and are ~25 MPa away from the weld for both R600 and R1500. In the NZ $\sigma^{m,tM+pM}$ has a maximum value of ~78 MPa and ~41 MPa for R600 and for R1500, respectively. This is surprising, because the higher temperature level during welding for R1500 should not result in lower thermal misfit plus plastic misfit residual stresses in the matrix of the NZ compared to that for R600. This result clearly reveals that the sample of unreinforced alloy is not adequate to derive the absolute unstrained reference parameter $d_0^{m,a}$, because it yields unreasonable results and leads to significant errors in the final stress calculation.

Fig. 7(a) shows that the profiles of $\sigma^{m,tM+pM}$ calculated using $d_0^{p,a}$ are symmetrical. For R600, the value of $\sigma^{m,tM+pM}$ calculated using $d_0^{p,a}$ is ~76 MPa away from the weld center, and it decreases slightly to ~72 MPa at the weld center. For R1500, $\sigma^{m,tM+pM}$ is ~83 MPa away from the weld center and has almost the same value at the weld center as R600.

It can be seen that the thermal misfit plus plastic misfit residual stresses in the matrix of the BM approximate to 80 MPa for both R600 and R1500. This value agrees very well with that in the 2124Al matrix of the 17 vol.% SiCp/2124Al composites in both natural aging and overaging tempers in previous studies [29,52]. This indicates that the thermal misfit plus plastic misfit residual stresses in the matrix of the BM are inherited from the T4 treatment and are not much affected by the welding thermal exposure. This is easy to understand because the modification of the pre-existing thermal misfit plus plastic misfit residual stresses (caused by the T4 treatment in this study) only occurs when the temperature is high enough. For instance, Bouafia et al. [53] showed that the von Mises stress in the matrix did not exceed the yield strength of the matrix in the SiCp/Al composite that had experienced 300 °C temperature drop and was then reheated with a 300 °C temperature rise. In such a case, the thermal misfit plus plastic misfit residual stresses in the matrix will not be modified because no plastic deformation occurs [52].

The thermal misfit plus plastic misfit residual stresses in the matrix of the NZ for R1500 are nearly equal to that for R600. The phenomenon is probably related to variations in the mechanical behavior of the matrix due

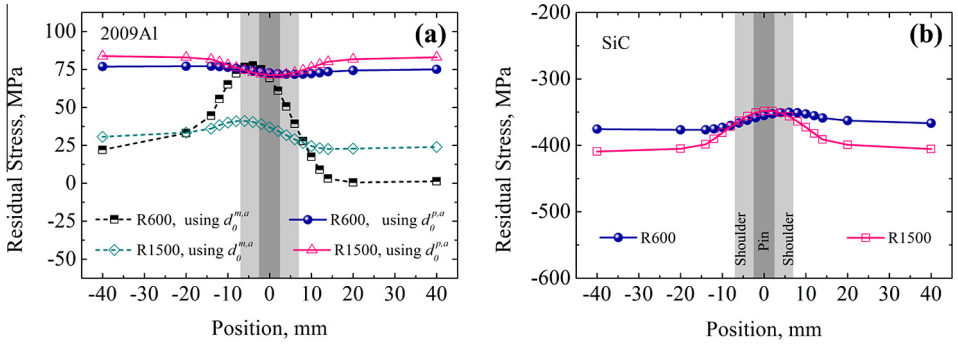

Fig. 7. Comparison of the thermal misfit plus plastic misfit residual stresses across the welds for R600 and R1500: (a) in the 2009Al matrix, both the residual stresses that were calculated via the $d_0^{m,a}$ and $d_0^{p,a}$ (using the equilibrium conditions) are presented; (b) in the SiC reinforcement.

to the change of precipitation state under the FSW thermal exposure. The R1500 sample experienced higher temperature exposure, and consequently is prone to generate higher thermal misfit plus plastic misfit residual stresses, however, higher temperature exposure usually produces welds with lower yield strength for age-hardened alloys [54]. During the cooling stage, plastic deformation in the matrix caused by the mismatch of the CTE is favored for MMC weld with softer matrix. Compared to that for R600, a larger amount of thermal misfit plus plastic misfit residual stresses in the matrix of the weld for R1500 may be relaxed through the plastic deformation, resulting in the thermal misfit plus plastic misfit residual stresses in the weld of R1500 being of almost the same magnitude as that of R600.

Fig. 7(b) shows that $\sigma^{p,tM+pM}$ is about −370 MPa away from the weld, and it increases slightly to about −350 MPa at the weld center. For R1500, $\sigma^{p,tM+pM}$ is ~335 MPa away from the weld and it increases to almost the same value at the weld center.

4.2.2. The elastic mismatch residual stress

Fig. 8(a) shows that the profile of the elastic mismatch stress $\sigma_L^{m,eM}$ is approximately M-shaped, whereas Fig. 8(b) shows that the profile of $\sigma_L^{p,eM}$ is approximately W-shaped. Fig. 8(c) shows that the profile of $\sigma_T^{m,eM}$ has three peaks, whereas Fig. 8(d) shows that the profile of $\sigma_T^{p,eM}$ has three troughs. Fig. 8(e) shows that the profile of $\sigma_N^{m,eM}$ is inversely V-shaped, whereas Fig. 8(f) shows that the profile of $\sigma_N^{p,eM}$ is V-shaped.

Fig. 8 clearly shows that the profiles of the elastic mismatch residual stress in the reinforcement $\sigma_L^{p,eM}$, $\sigma_T^{p,eM}$ and $\sigma_N^{p,eM}$ are opposite to those in the matrix $\sigma_L^{m,eM}$, $\sigma_T^{m,eM}$ and $\sigma_N^{m,eM}$, revealing the load transfer from the matrix to the reinforcement. Furthermore, the total variation of $\sigma_L^{p,eM}$ is significantly greater than that of $\sigma_T^{p,eM}$ and $\sigma_N^{p,eM}$. This is partly attributed to the fact that the SiC particles tended to align along the *N* direction in the center of the NZ and the load transfer from the matrix to the reinforcement is greater along the long axis of the particle than that along the short axis [29].

The total variation of the elastic mismatch residual stress in the reinforcement $\sigma_L^{p,eM}$, $\sigma_T^{p,eM}$ and $\sigma_N^{p,eM}$ is about 4.9 times of that in the matrix $\sigma_L^{m,eM}$, $\sigma_T^{m,eM}$ and $\sigma_N^{m,eM}$, i.e. ~260 MPa vs. ~53 MPa, ~295 MPa vs. ~60 MPa, and ~426 MPa vs. ~87 MPa, which exactly correlates to the ratio of the volume fraction between the 2009Al matrix and SiC reinforcement in the 17 vol.% SiCp/2009Al composite, as expected.

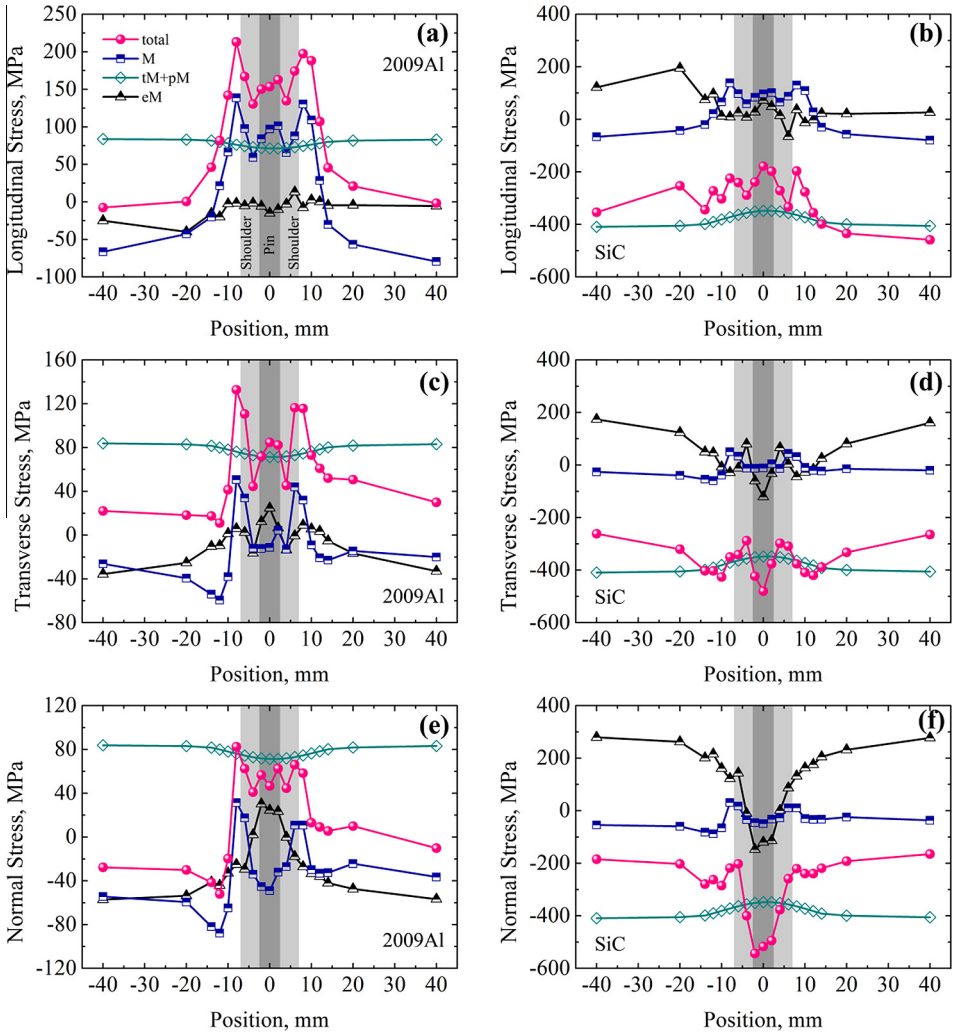

Fig. 8. The profiles of σ_i^M, σ_i^{eM}, $\sigma^{\beta,tM+pM}$ and $\sigma_i^{\beta,\text{total}}$ in both the 2009Al matrix and SiC reinforcements for R1500 across the weld.

4.2.3. The macroscopic and total residual stresses

Fig. 8(a) shows that the profile of macroscopic residual stress σ_L^M is approximately M-shaped, in agreement with previous works [19,55]. The profile of the resulting total stress $\sigma_L^{m,\text{total}}$ is similar to that of σ_L^M, approximately M-shaped. The peak stresses of both σ_L^M and $\sigma_L^{m,\text{total}}$ are just beyond the shoulder radius. The total variations of σ_L^M and $\sigma_L^{m,\text{total}}$ are ~218 MPa and ~221 MPa, respectively. In addition, it can be seen that the L components of σ_i^M and $\sigma_i^{m,\text{total}}$ are significantly larger than the T and N components of σ_i^M and $\sigma_i^{m,\text{total}}$, as shown in Fig. 8(a), (c) and (e).

Fig. 8(a) shows that the maximum σ_L^M is ~139 MPa, reaching up to ~40% of the effective yield strength of the 17 vol.% SiCp/2009Al-T4 composite, which is ~344 MPa at ambient temperature [8]. This seems to indicate that the total level of residual stress in MMCs is low (e.g. smaller than 40%). However, the plastic, fatigue and corrosion behaviors of the MMCs containing low contents of reinforcement (e.g. below 30 vol.%) are predominately determined by the behavior of the matrix. It is therefore more appropriate to use the ratio of the maximum L component of the total residual stress to the yield strength of the matrix for assessing the level of the residual stress.

Taking this into account the maximum value of $\sigma_L^{m,\text{total}}$ is ~213 MPa as shown in Fig. 8(a), reaching up to ~69% of the yield strength of the 2009Al-T4 alloy that is ~ 310 MPa at ambient temperature. It should be noted that the yield strength of the weld is usually lower than that of the BM. Ni et al. [9] reported that the micro-hardness of the NZ and HAZ of FSW weld of 17 vol.% SiCp/2009Al-T351 composite was ~80% and ~65% of that of the BM. Generally, the yield strength is linearly related to the hardness, and thus it is reasonable to assume that the yield strengths of the NZ and HAZ are ~80% and ~65% of that of the BM. Taking this into account the ratio of the maximum L component of the total residual stress to the yield strength of the matrix in the FSW MMC welds may reach up to 100%.

Fig. 8(a), (c) and (e) shows that in the matrix of the FSW MMC welds, the profiles and total variations of the L, T and N components of the total residual stress are close to those of the macroscopic residual stress, as one would expected. The variations of the L, T and N components of the macroscopic residual stress are greater than those of elastic mismatch, thermal misfit plus plastic misfit residual stresses in the matrix. It is known that the main material properties that influence the development of the residual stress in the welds include thermal conductivity, heat capacity, CTE, elastic constants and plasticity [56]. Because all these material properties of the MMCs with low content of reinforcement (e.g. below 30 vol.%) are close to those of the metal matrix rather than the reinforcement, it is clear that the variations of the total residual stress in the metal matrix of the FSW MMC welds are dominated by the macroscopic residual stress in the matrix. The thermal misfit plus plastic misfit residual stresses in the matrix only increase, almost homogeneously, the level of tensile residual stress, whereas the elastic mismatch residual stress in the matrix has relatively small effect on the total residual stress.

It is quite surprising that unlike the status in the matrix, in the reinforcement of the FSW MMC welds, as shown in Fig. 8(b), (d) and (f), the profiles of the L, T and N components of the total residual stress $\sigma_i^{p,\text{total}}$ are very different from the usual profiles of the macroscopic residual stress introduced by welding. The total variation of the N component of the total residual stress $\sigma_N^{p,\text{total}}$ is greater than that of the L and T components. Fig. 8(f) shows that the profiles of $\sigma_N^{p,eM}$ and $\sigma_N^{p,\text{total}}$ are similar and they are V-shaped, with their lowest values located at the center of the weld. The lowest value of $\sigma_N^{p,\text{total}}$ is about −543 MPa with the total variation of $\sigma_N^{p,\text{total}}$ is about 378 MPa. These results show that the profiles and the total variations of the L, T and N components of the total residual stress in the reinforcement are determined by those of the elastic mismatch residual stress. The variations of the L, T and N components of the elastic mismatch residual stress are greater than those of the macroscopic, thermal misfit plus plastic misfit residual stresses in the reinforcement. This phenomenon is different from that in the quenched MMCs in reference [29] where the macroscopic residual stress determines the profiles and the variation of the total residual stress in the reinforcement.

This phenomenon is probably caused by the following major facts. First, the SiC particles in the NZ flowed and rotated in the matrix driven by the stirring effect of the welding tool. Some SiC particle clusters were broken up and the particles tended to align along the N direction in the center of the NZ, as shown in Figs. 2 and 3. These changes can increase the load transfer from the matrix to the reinforcement [29,57]. Second, severe plastic deformation in the matrix of the NZ due to the stirring effect of the welding tool causes the interfacial compounds to fall off the SiC particles. This leads to formation of more clean interface of metallurgical bonding between the SiC particles and the 2009Al matrix [34], which in turn increases the load transfer from the matrix to the reinforcement in the NZ [57]. These facts reflect the complexity involved in FSW MMC welds. In order to obtain greater insight into the development of the elastic mismatch residual stress, as well as the other residual stresses during the FSW process, advanced models like multi-scale finite element model may be a promising tool. This work is ongoing.

The thermal misfit plus plastic misfit residual stresses determine the base level of the total residual stress in the reinforcement. The macroscopic residual stress in the reinforcement has relatively small effects on the total residual stress. This is probably due to the fact that the reinforcements are discontinuously distributed and their content is low, 17 vol.% in this study.

4.3. Effects of the rotation rate

Fig. 9 compares the profiles of total residual stress $\sigma_i^{\beta,\text{total}}$ between R600 and R1500. It indicates that raising the rotation rate has a small effect on the basic profiles of $\sigma_i^{\beta,\text{total}}$, but increases the width of the profiles of $\sigma_i^{\beta,\text{total}}$. For instance, Fig. 9(a), (c) and (e) shows that raising the rotation rate increases the width of the regions of the total residual stress in the matrix $\sigma_i^{m,\text{total}}$ with higher tensile values in agreement with previous investigations [15,58]. This phenomenon is mainly caused by the variation in temperature distribution: higher rotation rates introduces higher temperatures, thus the widths of the profiles of $\sigma_i^{\beta,\text{total}}$ become larger [15,39,58].

In the reinforcement, when increasing the rotation rate, the widths of the regions of the total residual stress increase

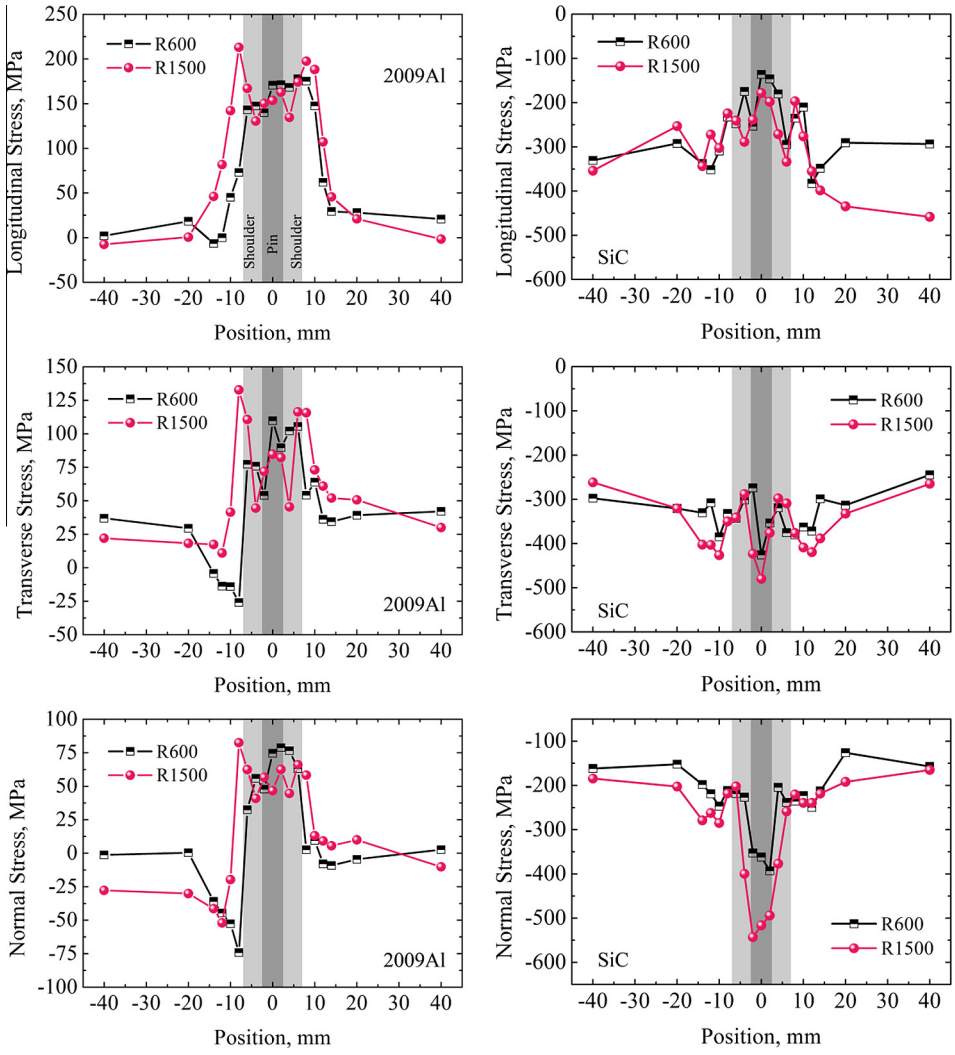

Fig. 9. Comparison of the total residual stress for R600 and R1500: (a) *L*, (c) *T* and (e) *N* components in the 2009Al matrix, (b) *L*, (d) *T* and (f) *N* components in the SiC reinforcements.

slightly. Meanwhile, a significant increase of the absolute magnitude in the total residual stress along the *N* direction occurs as depicted in Fig. 9(f). This is probably because: first, the onion structure formed in the NZ for R1500 and more SiC particles aligned along the *N* direction for R1500 compared to R600, as shown in Figs. 2 and 3; second, raising the rotation rate can increase the amount of newly formed clean reinforcement/matrix interfaces. These changes lead to a significant increase in the load transfer from the matrix to the reinforcement along the *N* direction. Since the total residual stress is determined by the elastic mismatch residual stress in the reinforcement, hence, the absolute magnitude of the total residual stress along the *N* direction in the reinforcement increases with increasing the rotation rate, as depicted in Fig. 9(f).

4.4. The macroscopic residual stresses in the MMCs and unreinforced alloys

It is interesting to compare the macroscopic residual stresses in the FSW MMCs and the FSW unreinforced alloys. Fig. 10 shows the quantitative comparison in the macroscopic residual stresses between the FSW MMCs and unreinforced alloys that are taken from literatures [18,20,40,59]. It can be seen that both the profiles and values of the macroscopic residual stresses in the FSW MMCs are close to those in the FSW unreinforced alloys. This is not surprising because MMCs with low contents of

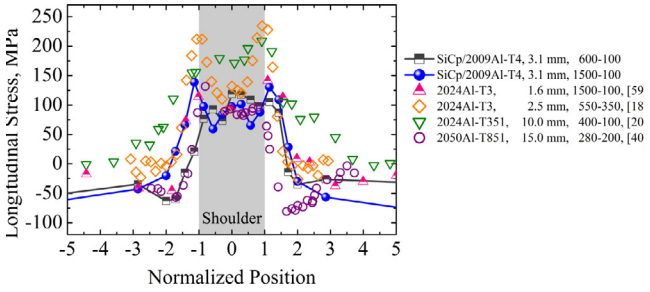

Fig. 10. Comparison in the macroscopic residual stress between the FSW MMCs and unreinforced alloys that are taken from literatures [18,20,40,59]. The 'normalized position' is calculated by dividing the real distance away from the weld center by the shoulder radius. "SiCp/2009Al-T4, 3.1 mm, 600–100" means the material is SiCp/2009Al-T4, 3.1 mm in thickness, the rotation rate is 600 rpm, and the advancing speed is 100 mm/min.

reinforcement (e.g. the volume fraction is 17% in this study) behave like the unreinforced alloys.

5. Conclusions

This study presents a new method for ascertaining the residual stress in MMC welds. In order to determine the macroscopic and microscopic (including elastic mismatch, thermal misfit and plastic misfit) residual stresses in MMC welds, neutron diffraction data are employed with Hooke's law and the equilibrium conditions of the microscopic residual stresses are imposed. As an example, the residual stress in the FSW welds of 17 vol.% SiCp/2009Al-T4 plates were investigated. The conclusions can be summarized as follows:

(1) In the matrix, the profiles and total variations of the L, T and N components of the total residual stress are determined by those of the macroscopic residual stress in the matrix. The elastic mismatch residual stress has a relatively minor effect on the total residual stress in the matrix.
(2) The profiles of the L, T and N components of the total residual stress in the reinforcement are totally different from those in the matrix. The L component of the total residual stress in the matrix in particular has a typical M-shape, whereas that in the reinforcement has three peaks. The N component of the total residual stress in the matrix has an M-shape, whereas that in the reinforcement has an obvious V-shape.
(3) In the reinforcement, the profiles and total variations of the L, T and N components of the total residual stress are dominated by those of the elastic mismatch residual stress. This reveals a significant load transfer from the matrix to the reinforcement. The macroscopic residual stress has a relatively minor effect on the total residual stress in the reinforcement.
(4) For both the matrix and the reinforcement, the thermal misfit plus plastic misfit residual stresses in the BM are inherited from the T4 treatment, whereas those in the weld are generated due to FSW. The thermal misfit plus plastic misfit residual stresses in the matrix moved the total residual stress into tensile by about 80 MPa for both R600 and R1500. The thermal misfit plus plastic misfit residual stresses determine the base level of the total residual stress in the reinforcement.
(5) The maximum total residual stress in the matrix of R1500 reached up to ~69% of the yield strength of the 2009Al-T4 alloy. Raising the rotation rate has small effects on the basic profiles of the total residual stress, apart from increasing the width of the profiles. When increasing the rotation rate, the highest stress of the L component of the total residual stress in the matrix increases, whereas the lowest value of the N component of the total residual stress in the matrix decreases.

Acknowledgments

The authors gratefully acknowledge support from the National Natural Science Foundation of China under Grant No. 51401219 and the National Basic Research Program of China under Grant No. 2012CB619600. The authors are very grateful to the staff of FRM II Garching, Germany for their kind support of the experiments on their sites. The authors would like to thank Prof. Gaspar González-Doncel for his helpful discussions and comments.

References

[1] D. Storjohann, O.M. Barabash, S.S. Babu, S.A. David, P.S. Sklad, E.E. Bloom, Metall. Mater. Trans. A 36A (2005) 3237.
[2] W.B. Lee, C.Y. Lee, M.K. Kim, J.I. Yoon, Y.J. Kim, Y.M. Yoen, S.B. Jung, Compos. Sci. Technol. 66 (2006) 1513.
[3] R.A. Prado, L.E. Murr, D.J. Shindo, K.F. Soto, Scr. Mater. 45 (2001) 75.
[4] Z.Y. Ma, A.H. Feng, B.L. Xiao, J.Z. Fan, L.K. Shi, in: T. Chandra, K. Tsuzaki, M. Militzer, C. Ravindran (Eds.), THERMEC 2006, Pts 1–5, vol. 539–543. 2007. p. 3814.
[5] A.H. Feng, B.L. Xiao, Z.Y. Ma, Compos. Sci. Technol. 68 (2008) 2141.
[6] T.W. Nelson, H. Zhang, T. Haynes, in: Proc. 2nd Int. Symposium on Friction Stir Welding, Gothenburg, Sweden, 2000.
[7] T. Prater, A. Strauss, G. Cook, B. Gibson, C. Cox, J. Mater. Eng. Perform. 22 (2013) 1807.
[8] D. Wang, Q.Z. Wang, B.L. Xiao, Z.Y. Ma, Mater. Sci. Eng., A 589 (2014) 271.
[9] D.R. Ni, D.L. Chen, D. Wang, B.L. Xiao, Z.Y. Ma, Mater. Sci. Eng., A 608 (2014) 1.
[10] D. Wang, B.L. Xiao, D.R. Ni, Z.Y. Ma, Acta Metall. Sin. (Engl. Lett.) 27 (2014) 816.
[11] N. Kumar, R.S. Mishra, J.A. Baumann, A Brief Introduction to FSW, in: N. Kumar, R.S. Mishra, J.A. Baumann (Eds.), Residual Stresses in Friction Stir Welding, Butterworth-Heinemann, Boston, 2014, p. 5 (Chapter 2).
[12] P. Staron, M. Kocak, S. Williams, Appl. Phys. A 74 (2002) S1161.
[13] M.A. Sutton, A.P. Reynolds, D.Q. Wang, C.R. Hubbard, J. Eng. Mater. Technol. -Trans. ASME 124 (2002) 215.
[14] M. Peel, A. Steuwer, M. Preuss, P.J. Withers, Acta Mater. 51 (2003) 4791.
[15] A.P. Reynolds, W. Tang, T. Gnaupel-Herold, H. Prask, Scr. Mater. 48 (2003) 1289.
[16] P. Staron, M. Kocak, S. Williams, A. Wescott, Physica B 350 (2004) E491.
[17] A. Steuwer, M.J. Peel, P.J. Withers, Mater. Sci. Eng., A 441 (2006) 187.
[18] H.J.K. Lemmen, R.C. Alderliesten, R.R.G.M. Pieters, R. Benedictus, J.A. Pineault, J. Aircr. 47 (2010) 1570.
[19] W. Woo, Z. Feng, X.L. Wang, S.A. David, Sci. Technol. Weld. Join. 16 (2011) 23.
[20] F. Cioffi, J.I. Hidalgo, R. Fernandez, T. Pirling, B. Fernandez, I. Puente Orench, P. Rey, G. Gonzalez-Doncel, Acta Mater. 74 (2014) 189.
[21] P.J. Withers, Rep. Prog. Phys. 70 (2007) 2211.
[22] D.R. Ni, D.L. Chen, B.L. Xiao, D. Wang, Z.Y. Ma, Int. J. Fatigue 55 (2013) 64.
[23] C.D.M. Liljedahl, J. Brouard, O. Zanellato, J. Lin, M.L. Tan, S. Ganguly, P.E. Irving, M.E. Fitzpatrick, X. Zhang, L. Edwards, Int. J. Fatigue 31 (2009) 1081.
[24] G. Biallas, Int. J. Fatigue 50 (2013) 10.
[25] R.M.F. Paulo, P. Carlone, R.A.F. Valente, F. Teixeira-Dias, G.S. Palazzo, Thin Walled Struct. 74 (2014) 184.
[26] P.S. Prevey, J.T. Cammett, Int. J. Fatigue 26 (2004) 975.
[27] T.S. Jun, F. Rotundo, L. Ceschini, A.M. Korsunsky, in: H.S. Lee, I.S. Yoon, M.H. Aliabadi (Eds.), Advances in Fracture and Damage Mechanics VII, vol. 385–387, 2008, p. 517.
[28] A. Pirondi, L. Collini, Int. J. Fatigue 31 (2009) 111.
[29] M.E. Fitzpatrick, M.T. Hutchings, P.J. Withers, Acta Mater. 45 (1997) 4867.
[30] P.J. Withers, M. Preuss, A. Steuwer, J.W.L. Pang, J. Appl. Crystallogr. 40 (2007) 891.

[31] A.R. Denton, N.W. Ashcroft, Phys. Rev. A 43 (1991) 3161.
[32] D.R. Ni, D.L. Chen, D. Wang, B.L. Xiao, Z.Y. Ma, Mater. Des. 51 (2013) 199.
[33] D. Wang, B.L. Xiao, Q.Z. Wang, Z.Y. Ma, Mater. Des. 47 (2013) 243.
[34] D. Wang, B.L. Xiao, Q.Z. Wang, Z.Y. Ma, J. Mater. Sci. Technol. 30 (2014) 54.
[35] M. Hofmann, R. Schneider, G.A. Seidl, J. Rebelo-Kornmeier, R.C. Wimpory, U. Garbe, H.G. Brokmeier, Physica B 385–86 (2006) 1035.
[36] A. Paradowska, T.R. Finlayson, J.W.H. Price, R. Ibrahim, A. Steuwer, M. Ripley, Physica B 385–386 (2006) 904.
[37] C. Randau, U. Garbe, H.G. Brokmeier, J. Appl. Crystallogr. 44 (2011) 641.
[38] J.H. Yan, M.A. Sutton, A.P. Reynolds, Sci. Technol. Weld. Join. 10 (2005) 725.
[39] A. Steuwer, S.J. Barnes, J. Altenkirch, R. Johnson, P.J. Withers, Metall. Mater. Trans. A 43A (2012) 2356.
[40] G. Pouget, A.P. Reynolds, Int. J. Fatigue 30 (2008) 463.
[41] L. Fratini, S. Pasta, A.P. Reynolds, Int. J. Fatigue 31 (2009) 495.
[42] D.J. Hughes, M.N. James, D.G. Hattingh, P.J. Webster, J. Neutron Res. 11 (2003) 289.
[43] S. Ganguly, L. Edwards, M.E. Fitzpatrick, Mater. Sci. Eng., A 528 (2011) 1226.
[44] Y.E. Ma, P. Staron, T. Fischer, P.E. Irving, Int. J. Fatigue 33 (2011) 1417.
[45] P. Rodrigo, P. Poza, V. Utrilla, A. Urena, J. Alloys Compd. 479 (2009) 451.
[46] S.M. Xu, X.M. Deng, Acta Mater. 56 (2008) 1326.
[47] W.B. Pearson, A Handbook of Lattice Spacings and Structures Of Metals and Alloys, Pergamon Press, London, 1958.
[48] W.D.J. Callister, D.G. Rethwisch, Materials Science and Engineering: An Introduction, John Wiley & Sons Inc, Hoboken, 2010.
[49] D.P. Field, T.W. Nelson, Y. Hovanski, K.V. Jata, Metall. Mater. Trans. A 32 (2001) 2869.
[50] P.B. Prangnell, C.P. Heason, Acta Mater. 53 (2005) 3179.
[51] T. Gnaeupel-Herold, J. Appl. Crystallogr. 45 (2012) 573.
[52] M.E. Fitzpatrick, P.J. Withers, A. Baczmanski, M.T. Hutchings, R. Levy, M. Ceretti, A. Lodini, Acta Mater. 50 (2002) 1031.
[53] F. Bouafia, B. Serier, B.A.B. Bouiadjra, Comp. Mater. Sci. 54 (2012) 195.
[54] Z. Zhang, B.L. Xiao, Z.Y. Ma, Acta Mater. 73 (2014) 227.
[55] W. Woo, V. Em, P. Mikula, G.-B. An, B.-S. Seong, Mater. Sci. Eng., A 528 (2011) 4120.
[56] G. Totten, M. Howes, T. Inoue, Handbook of residual stress and deformation of steel, ASM Int., 2002.
[57] R. Mitra, Y.R. Mahajan, Bull. Mater. Sci. 18 (1995) 405.
[58] A. Steuwer, D.G. Hattingh, M.N. James, U. Singh, T. Buslaps, Sci. Technol. Weld. Join. 17 (2012) 525.
[59] W.T. Han, F.R. Wan, G. Li, C.L. Dong, J.H. Tong, Sci. Technol. Weld. Join. 16 (2011) 453.